The elastic behavior of a rubber-like material for composite glass

Silvia Briccoli Bati[1], Mario Fagone[1], Giovanna Ranocchiai[1]

[1]*Department of Costruzioni, University of Florence, Italy*
E-mail: *silvia.briccolibati@unifi.it*
mario.fagone@unifi.it
giovanna.ranocchiai@unifi.it

Keywords: rubberlike, hyperelastic behavior, inverse analysis.

SUMMARY. This paper is devoted to the mechanical characterization of the elastic behavior of thin sheets of a commercial Poly Vinyl Butyral (PVB) at room temperature. Foils of PVB are often used as interlayer in the laminated glass. Their elastic properties were investigated by displacement controlled tensile tests performed both on slender and on stocky samples. The elastic behavior was schematized by some hyperelastic models whose constitutive parameters was identified fitting the experimental results.

1 INTRODUCTION

Poly Vinyl Butyral (PVB) is a thermoplastic amorphous polymer characterized by long, branched and geometrically random polymer chains. Even if its mechanical characteristics strongly depends on the additives used during the industrial manufacture, its glass transition temperature is generally about the room temperature. The high level of deformation that can be reached by the material until failure is enabled by its macromolecular network structure, which nature brings a stress-strain behaviour that is primarily governed by changes in configurational entropy as the randomly-oriented molecular network becomes preferentially-oriented with stretching. PVB is often used as interlayer in practical applications of the structural laminated glass as a secondary structure. Its thermo-visco-elastic behavior and the adhesion between the glass and the interlayer strongly influence the mechanical behavior of the laminated glass both in normal working and in post-crack conditions. In particular, in the post crack condition, once the glass is broken, the polymeric interlayer of the composite is able to produce a large variety of equilibrium configurations and of ductility resorts, so that the knowledge of its mechanical properties is crucial in the evaluation of safety of this kind of structures or of structural elements.

In this paper only the macroscopic elastic behavior of foils of a commercial PVB at room temperature is investigated. Displacement driven tensile tests were performed else on slender and on stocky samples of thin sheets of PVB in order to induce in the material uniform uniaxial stress and not uniform biaxial stress states. The latest is due, in the stocky samples, to the confinement produced by the fish plates so that, in the experiments, a particular attention was paid to guarantee a good adhesion of the grasps to the plastic sheet. The experiments performed on the slender samples was already presented in [1] and are reported in the present paper for completeness.

The elastic behavior of PVB is modeled by some selected well known constitutive models [2], [3], [4], [5] that seems able to describe the elastic behavior of the material. The mechanical parameters defining these models have been determined by an inverse analysis, fitting, in the least square sense, the experimental results.

2 TENSILE TESTS

2.1 *Specimens*

The shape and dimensions of the specimens used in the tensile tests are reported in figure 1. All the specimens was made of a foil of PVB having a nominal thickness of 0.76 mm. In all the tests the displacements of the nodes of the grid drawn in the central part of the specimens was recorded for all the load steps. The shape and dimensions of the specimens was defined in order to obtain different shape ratios of the monitored zone. In particular we used two types of slender specimens, (a) and (b) in figure 1, and two types of stocky specimens, (c) and (d) in figure 1, having different aspect ratio.

Shape and dimensions of the specimens of type (a) in figure 1 were defined observing, as far as possible, the prescriptions of EN ISO 527-2. Particularly, the length of the specimens was chosen as to permit the desired strain to fulfill in the workspace of the press and to be performed by the jack; the shape was such that the zone of the specimen assigned for the mapping of deformations was initially long twice the width. The bone-shaped specimen prevents the sliding of material within the grasps and the rupture in correspondence of the constraint. In the tests the specimen was doubled in the direction of the length so as to grasp only the doubled side. Sand paper was interposed between the iron plates and the polymer foils in order to increase friction. On the other side of the bone-shaped specimen, one cylinder with diameter of 10 mm was devoted to restrain the specimen.

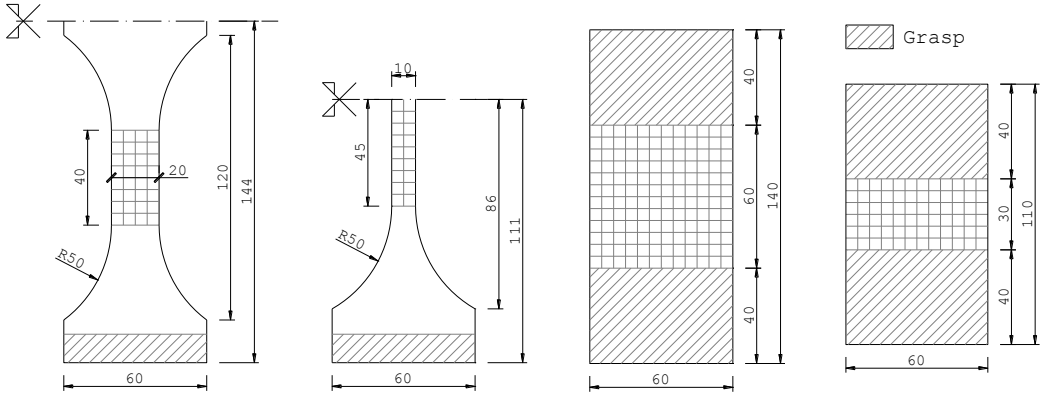

Figure 1: Shape and dimensions of samples in tensile tests. Lengths in mm.

In the tensile tests performed on specimens of type (a) we was not able to reach the rupture of the material elongating the specimen in the workspace of the press. In order to produce the break of one PVB, a specimen of type (b) was used. For this reason the enlargement at the bottom of the specimen was no more produced, relying on the small confinement produced by the contact with the cylinder. Consequently, the doubled specimen was half bone shaped. Moreover, the width of the strip was reduced to 10 mm, as to obtain a maximum load apt to the capability of the used load cell.

In the tensile tests, a substantially uniaxial stress state was induced in the marked zone of the specimens of both type (a) and type (b). In order to produce, at least locally, a biaxial stress state, specimens of types (c) and (d) was used. Also in this case the maximum length of these specimens was chosen as to permit the desired deformation to fulfill in the workspace of the press. Moreover,

as the load cell of adequate precision could be used, these samples was not doubled in the direction of the length. Both the upper and the lower side of the specimens was grasped in order to confine the specimens and to induce a biaxial stress state at least in the areas close to the grasps.

2.2 *Displacement controlled tests*

The specimens were hung by means of the grasp to a load cell which was fixed to the screw jack that was in turn connected to the test frame. In view of the different expected maximum load, a load cell having 0.1 N of resolution and 500 N of measuring range was used for the slender specimens (types (a) and (b) in Figure 1), while a load cell having 2 N of resolution and 5000 N of measuring range was used for the stocky specimens (types (c) and (d) in Figure 1). While the bottom of the specimen was fixed, the displacement in correspondence of the top was measured with a wire displacement sensor. Both load and displacement data were recorded with a data logger. The relative displacements between the node of the grid drawn in the central area of the specimens (see Figure 1) was taken with a camera fixed on a tripod.

The tests were performed imposing fixed displacement steps and allowing relaxation to occur in order to (conventionally) reach the elastic deformations. The relaxation phases between the displacements step, initially established in 5 min [6], were successively increased to 20 min because of the great amount of viscous deformations and of the long relaxation time exhibited by the material. The length of the relaxation phase is obviously conventional, as it is impossible, in laboratory time, to obtain the full relaxation of viscous phenomena and the pure elastic deformation.

The following displacement controlled tests was performed (see Figure 1):

- 3 tests on specimens of type (a)
- 1 test on a specimen of type (b)
- 2 tests on specimens of type (c)
- 3 tests on specimens of type (d)

The global data of the tests are reported in Table 1. The letter in the denomination refers to the kind of specimen described in Figure 1.

Table 1: Displacement controlled tests.

Specimen denomination	Average temperature	Average relative humidity	Displacement step		Number of total steps	Relaxation time
			Displacement	Rate		
	[°C]	[%]	[mm]	[mm/min]		[min]
a01	23-24	/	10	10	27	5
a02	26.0	/	10	10	28	20
a03	23.0	/	10	10	29	20
b01	24.3	/	10	10	25	20
c01	19.1	49.5	20	10	5	20
c02	19.1	49.5	20	10	8	20
d01	19.0	50.0	10	10	6	20
d02	18.2	58.0	10	10	6	20
d03	18.2	58.0	10	10	6	20

In Figure 2 the time-load diagram of specimen *b01* is reported and time-load diagrams of some relaxation phases are superimposed. In Figure 3 it is reported the stretch vs. nominal stress diagram of the equilibrium points corresponding to the end of the relaxation phases. In order to compare all the tests, we reported the nominal stress, in the direction of the load, and the stretch

(ratio between the current and the initial lengths) calculates for the middle point of the grid drawn in the specimens. It is apparent that small variation of room temperature produce large differences of deformability of the material. Moreover, as expected, the curves in Figure 3 that refers to the "confined" tests are more stiff than the ones that refers to slender specimens.

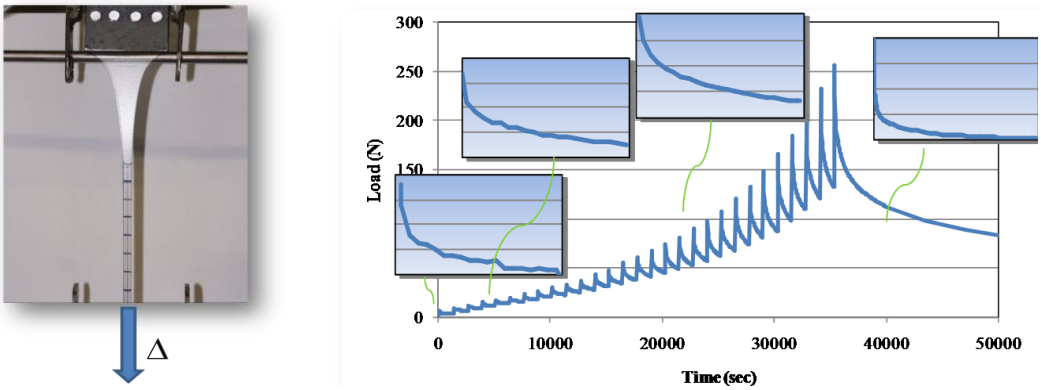

Figure 2: Time vs. Load diagram of the specimen *b01*.

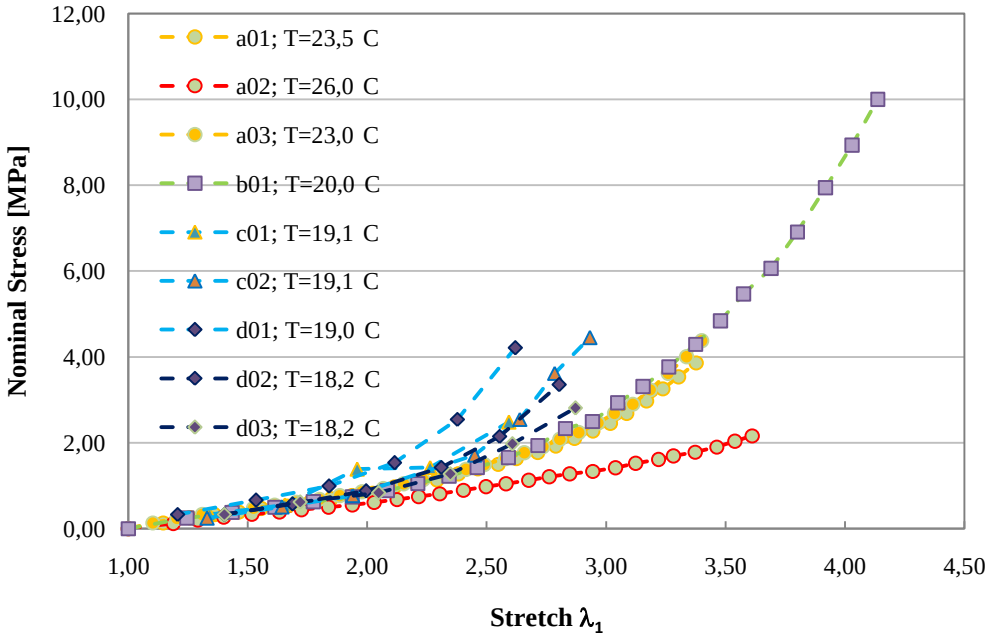

Figure 3: Stretch vs. (conventional) elastic Nominal Stress

3 HYPERELASTIC CONSTITUTIVE MODELS

From the tests reported in the previous section it is apparent that PVB exhibits a non-linear visco-elastic behaviour. Although the viscous part of the material behaviour may be significant in

many practical utilizations, here we restrict ourselves only to the modelling of the elastic part of its mechanical behaviour that is in any case crucial in many practical application.

In the past decades a very large number of mechanical models for rubber-like materials have been developed on the basis of statistical mechanics treatments [7], [8], [9] and of a phenomenological approach [3], [10]. In particular, for the modelling of the constitutive behaviour of the examined PVB samples, we refer to hyperelastic constitutive models, so that we assume that a Helmoltz free energy ψ exists that rules the elastic part of the deformation process and that depends only on the local deformation. Thermal effects are not taken in account. Moreover we restrict to homogeneous materials and anisotropic behaviour, induced for example by Mullin's effects [11] are neglected, so that we assume that the symmetry group of the material is the full set of orthogonal transformations. Under this hypothesis, and according to the objective requirement, it is well known that the free energy depends only on a combination of the invariants of the right Cauchy-Green deformation tensor [12]

$$\psi = \overline{\psi}(I_1, I_2, I_3) = \tilde{\psi}(\lambda_1, \lambda_2, \lambda_3) \tag{1}$$

being

$$I_1 = tr(\mathbf{C}); \qquad I_2 = \frac{1}{2}\left((tr\boldsymbol{C})^2 - tr(\mathbf{C}^2)\right); \qquad I_3 = det(\boldsymbol{C}) = det(\boldsymbol{F})^2 = J^2 \tag{2}$$

$\lambda_1,\ \lambda_2,\ \lambda_3$ eigenvalues of the gradient of deformation tensor $\mathbf{F}$ (3)

$\mathbf{F}$ gradient of deformation tensor (4)

$\mathbf{C} = \mathbf{F}^{\mathrm{T}}\mathbf{F}$ right Cauchy-Green deformation tensor (5)

As it is apparent analyzing the results reported in [1] and according to literature, this kind of materials exhibit a weakly-compressible behaviour that is generally neglected. Thereby, many hyper-elastic constitutive models were originally developed with reference only to the first and the second invariants of the right Cauchy-Green deformation tensor (2), without explicit dependence on the Jacobian of the gradient of deformation that, as it is well known, measures the local volume change of the continuous. For near-incompressible materials the elastic free energy ψ is generally decomposed as follows

$$\psi = \omega\left(\overline{I}_1, \overline{I}_2\right) + U(J) \tag{6}$$

where $U(J)$ is a volume-changing term that depends on the determinant of the deformation gradient tensor (see (2)) and $\omega\left(\overline{I}_1, \overline{I}_2\right)$ is a volume-preserving term that depends on the first and second invariant of the unimodular right Cauchy-Green deformation tensor defined as follows [13]

$$\overline{\boldsymbol{C}} = \boldsymbol{J}^{-2/3}\boldsymbol{C} \tag{7}$$

$$\overline{I}_1 = tr\left(\overline{\mathbf{C}}\right) = I_1 I_3^{-\frac{1}{3}};\ \ \overline{I}_2 = \frac{1}{2}\left(\left(tr\overline{\boldsymbol{C}}\right)^2 - tr\left(\overline{\mathbf{C}}^2\right)\right) = tr\left(\overline{\mathbf{C}}^{-1}\right) = I_2 I_3^{-\frac{2}{3}};\ \overline{I}_3 = det\left(\overline{\boldsymbol{C}}\right) = 1 \tag{8}$$

From the Clausius-Plank inequality, enforcing explicitly the incompressibility constraint $\lambda_1\,\lambda_2\,\lambda_3 = 1$, standard arguments lead to the following well known expression for the components of the Cauchy stress tensor in a principal reference system

$$\sigma_i = \lambda_i \frac{\partial \omega\left(\overline{I}_1, \overline{I}_2\right)}{\partial \lambda_i} - p \tag{9}$$

being p the hydrostatic pressure that can be calculated from equilibrium consideration. In particular, let it be x_3 the axes orthogonal to the plane of the specimens described in the previous section. For all the described tests we have

$$\sigma_3 = 0 \longrightarrow p = \lambda_3 \frac{\partial \omega(\bar{I}_1, \bar{I}_2)}{\partial \lambda_3} \tag{10}$$

so that the other components of principal true stress assumes the following expressions

$$\begin{aligned} \sigma_1 &= \lambda_1 \frac{\partial \omega(\bar{I}_1, \bar{I}_2)}{\partial \lambda_1} - \lambda_3 \frac{\partial \omega(\bar{I}_1, \bar{I}_2)}{\partial \lambda_3} = \lambda_1 \frac{\partial \omega(\bar{I}_1, \bar{I}_2)}{\partial \lambda_1} - \frac{1}{\lambda_1 \lambda_2} \frac{\partial \omega(\bar{I}_1, \bar{I}_2)}{\partial \lambda_3} \\ \sigma_2 &= \lambda_2 \frac{\partial \omega(\bar{I}_1, \bar{I}_2)}{\partial \lambda_2} - \lambda_3 \frac{\partial \omega(\bar{I}_1, \bar{I}_2)}{\partial \lambda_3} = \lambda_2 \frac{\partial \omega(\bar{I}_1, \bar{I}_2)}{\partial \lambda_2} - \frac{1}{\lambda_1 \lambda_2} \frac{\partial \omega(\bar{I}_1, \bar{I}_2)}{\partial \lambda_3} \end{aligned} \tag{11}$$

while the components of the nominal stress with respect to a principal reference system can be expressed as follows

$$\begin{aligned} \pi_1 &= \lambda_1^{-1} \sigma_1 = \frac{\partial \omega(\bar{I}_1, \bar{I}_2)}{\partial \lambda_1} - \frac{1}{\lambda_1^2 \lambda_2} \frac{\partial \omega(\bar{I}_1, \bar{I}_2)}{\partial \lambda_3} \\ \pi_2 &= \lambda_2^{-1} \sigma_2 = \frac{\partial \omega(\bar{I}_1, \bar{I}_2)}{\partial \lambda_2} - \frac{1}{\lambda_1 \lambda_2^2} \frac{\partial \omega(\bar{I}_1, \bar{I}_2)}{\partial \lambda_3} \end{aligned} \tag{12}$$

The conditions that ensures admissible solution to physical problems in finite elasticity represent a very debated question. With reference to hyperelastic models, constitutive inequalities translate to conditions on the free energy, so that, for example, polyconvexity and coerciveness of the free energy ensure the existence of a solution of the boundary value problem [4], [12]. This condition does not conflict with non-uniqueness of the solution since, roughly speaking, it guarantees the existence of at least one local minimum of the functional to be minimized. On the other hand the existence of a solution for every boundary condition and for a general body force distribution may be unrealistic in some conditions, so that a functional that does not satisfy polyconvexity should not be ruled out a-priori. However, in the case of pure elastic process, the polyconvexity, that of course does not guarantees that the problem is well posed, may be a good mathematical tool to ensure the existence of a minimum of the free energy.

In order to model the elastic behaviour of PVB, in the present paper we consider the two classes of polynomial expressions for the free energy described in the following.

3.1 *Rivlin Saunders model*

The Rivlin Saunders model [2] represents a class of polynomial models and includes the Mooney-Rivlin and the neo-Hookean constitutive models. Its nearly-incompressible materials extension is

$$\omega_{RS}(\bar{I}_1, \bar{I}_2) = \sum_{i=0}^{m} \sum_{j=0}^{n} c_{ij} (\bar{I}_1 - 3)^i (\bar{I}_2 - 3)^j \tag{13}$$

Against its simplicity, the Rivlin Saunders model generally requires high order terms in the fitting of the typical S-shaped stress-strain relation of rubber-like materials. On the other hand, as it is well known, a large number of high order terms may lead to numerical stability problems. Moreover, the expression (13) is not poly-convex because of the terms $(\bar{I}_2 - 3)^j$ [4].

We considered expressions of the Rivlin-Saunders model (13) complete up to third order of the invariants, that contains the material constants explained in the first, second and third row of Tables 3 and 4, and containing fourth order of the eigenvalues of the unimodular deformation tensor (7) (fourth to seventh row of Tables 3 and 4). Furthermore, in order to analyze the influence of the terms depending only on the first invariant of $\overline{\boldsymbol{C}}$ in the fitting data procedure, we considered two enriched Money-Rivlin type expressions, that contains the material constants indicated in the eighth and ninth row of Tables 3 and 4).

The identification procedure of the material parameters of the polynomial elastic potential (13) leads to a linear least square problem. As far as the authors know, it does not exists any physical requirement that leads to a restriction on the sign of all the coefficients of the polynomial expression (13), except for the neo-Hookean and the Mooney-Rivlin expressions that need not negative coefficients. Anyway, a sufficient condition, but not of course necessary, for the Rivlin-Saunders free energy to have not negative values for a general deformation process, is that the coefficients c_{ij} be not negative so that, in the identification procedure, we referred to a linear least square problem with not negative solutions.

3.2 *Hartmann and Neff model [4]*

This constitutive model represents an extension of the previous polynomial model where the mixed terms are not included ($c_{ij} = 0$ for $i \neq j$) and the not polyconvex term $\left(\overline{I}_2 - 3\right)^j$ is substituted by $\left(\overline{I}_2{}^{3/2} - 3\sqrt{3}\right)^j$ that is instead poly-convex. Its expression is the following

$$\omega_{HN} = \alpha\left(\overline{I}_1{}^3 - 3^3\right) + \sum_{i=1}^{m} c_{i0}\left(\overline{I}_1 - 3\right)^i + \sum_{j=1}^{n} c_{0j}\left(\overline{I}_2{}^{3/2} - 3\sqrt{3}\right)^j \tag{14}$$

This potential is also coercive if $\alpha > 0$. Analogously to the Rivlin-Saunders model, and for the same motivations, the identification of the material parameters leads to a linear least square problem with non-negative solution (as explained, this final requirement ensures that the free energy is non-negative for all deformation processes) so that for the constitutive parameters we enforced the following constraints:

$$\alpha > 0, c_{i0} \geq 0, i = 1, \dots, m, c_{0j} \geq 0, j = 1, \dots, n \tag{15}$$

In order to analyze the performance (in terms of fitting capability for the experimental data reported in this paper) of the different terms in the constitutive model, we have considered expressions of (14) up to m=3 and n=2 (see Tables 3 and 4).

4 PARAMETERS IDENTIFICATION

The parameters defining the constitutive models described in the previous section have been calibrated to best fit, in the least square sense, the experimental data reported in section 2. Two different procedures was implemented in fitting the data relative to the tests performed on the slender and on the stocky specimens. In the monitored region of the slender specimens, whose marked with a grid in figure 1, the stress state can be assumed homogeneous and uniaxial so that, in the identification procedure, we considered the longitudinal stretch and nominal stress calculated, for all the load steps, in the middle point of the marked area. Instead, in the stocky samples, the stress (and the strain) state is biaxial and not homogeneous because of the confinement of the grasps. For this reason, in the fitting procedure, we referred to the displacement

of the node of the grid and to the total load measured for every displacement step.

As it is well known, the goal of the least squares technique is to find the set of (material) parameters $\underline{c} = [c_1 \;\; c_2 \;\; c_3 \;\; ... \;\; c_m]$ that minimizes the objective function that, for both the implemented procedures, can be expressed as follows

$$\min_{\underline{c}} \left\| \underline{f}(\underline{s}, \underline{c}) - \underline{P} \right\|_2^2 = \min_{\underline{c}} \sum_{i=1}^{n} \left(f(\underline{s}_i, \underline{c}) - P_i \right)^2 \tag{16}$$

The objective function is therefore defined as the squared norm of the difference between a vector $\underline{P}$ that is a measure of the load or of the stress in the specimens, and a vector $\underline{f}(\underline{s},\underline{c})$given by a function that evaluate the relevant measure of load (or stress) according to the chosen constitutive model (so that according to the vector of material constants $\underline{c}$) and to a measure of the deformation $\underline{s}$. The entries of equation (16) particularized for both kind of tests are described in Table 2.

Table 2: Description of the variables of the best fit procedure

	tests performed on the slender specimens (a) and (b) in figure 1	tests performed on the stocky specimens (c) and (d) in figure 1
P_i	nominal stress recorded in the i^{th} load step, calculated with reference to the central point of the monitored region of the specimen;	total load recorded by the load cell in the i^{th} load step;
s_i	longitudinal stretch measured in the i^{th} load step, calculated with reference to the central point of the monitored region of the specimen;	vector of displacements of the node of the grid drawn in the central area of the specimens, recorded in the i^{th} load step;
f	constitutive law (12) particularized according to the chosen model;	F.E. on purpose numerical code that take the nodal displacements and the constitutive parameters in input and returns, in output, the total load calculated according to the particular constitutive law
$\underline{c}$	vector of constitutive parameters;	vector of constitutive parameters;

The procedure used in fitting the data relative to the stocky specimens required the implementation of an on purpose Finite Element code.

The polynomial models described in the previous section, lead to a linear least square problem with non-negative solutions. The optimum set of the material constants (expressed in MPa) and the residual of the objective functions for all the considered particularizations are reported in Tables 3 and 4. It is apparent that higher order terms are not necessary to fit the experimental data with an acceptable care. Moreover, in many optimum sets summarized in Tables 3 and 4, a lot of terms depending on the second invariant of the unimodular deformation tensor are ineffective so that the terms depending on the first invariant appear predominant in the data fitting.

In table 5 it is reported the residual of the objective function evaluated using the optimum sets determined as previously described and referring to both the uniaxial and the confined tests data. It is apparent that the optimum sets determined with reference to a kind of test don't fit very well the data relative to the other kind of test.

Table 3: Material constants (in MPa) determined fitting the “uniaxial” tests.

	α	c_{10}	c_{01}	c_{20}	c_{11}	c_{02}	c_{30}	c_{21}	c_{12}	c_{03}	c_{40}	Res. (Sq. norm) [MPa^2]
$\omega_{RS-1I-2}$		0.3709	0.0									4.5e+1
$\omega_{RS-2I-5}$		0.0	0.1648	0.0014	0.0608	0.0						2.7e+1
$\omega_{RS-3I-9}$		0.0	0.1911	0.0	0.0500	0.0	0.0	0.0	0.0	0.0068		2.7e+1
$\omega_{RS-1D-1}$		0.3709										4.5e+1
$\omega_{RS-2D-3}$		0.1603	0.0	0.0174								2.7e+1
$\omega_{RS-3D-5}$		0.0	0.1648	0.0014	0.0608		0.0					2.7e+1
$\omega_{RS-4D-8}$		0.0	0.1648	0.0014	0.0608	0.0	0.0	0.0			0.0	2.7e+1
ω_{MR-4}		0.1603	0.0	0.0174			0.0					2.7e+1
ω_{MR-5}		0.1603	0.0	0.0174			0.0				0.0	2.7e+1
$\omega_{HN-m1-n0}$	0.0006	0.2006										2.8e+1
$\omega_{HN-m1-n1}$	0.0006	0.2006	0.0									2.8e+1
$\omega_{HN-m2-n0}$	5.0e-5	0.1627		0.0161								2.7e+1
$\omega_{HN-m2-n1}$	5.0e-5	0.1840	0.0	0.0044								2.7e+1
$\omega_{HN-m2-n2}$	5.0e-5	0.1572	0.0	0.0		0.0036						2.7e+1
$\omega_{HN-m3-n0}$	5.0e-5	0.1840		0.0044			0.0					2.7e+1
$\omega_{HN-m3-n1}$	5.0e-5	0.1840	0.0	0.0044			0.0					2.7e+1
$\omega_{HN-m3-n2}$	5.0e-5	0.1572	0.0	0.0		0.0036	0.0					2.7e+1

Table 4: Material constants determined fitting the “confined” tests

	α	c_{10}	c_{01}	c_{20}	c_{11}	c_{02}	c_{30}	c_{21}	c_{12}	c_{03}	c_{40}	Squared norm [MPa^2]
$\omega_{RS-1I-2}$		0.4615	0.0									1.6e+1
$\omega_{RS-2I-5}$		0.1141	0.0	0.0450	0.0	0.0						5.7e+0
$\omega_{RS-3I-9}$		0.1698	0.0	0.0243	0.0	0.0	0.0020	0.0	0.0	0.0		5.6e+0
$\omega_{RS-1D-1}$		0.4615										1.6e+1
$\omega_{RS-2D-3}$		0.1141	0.0	0.0450								5.7e+0
$\omega_{RS-3D-5}$		0.1698	0.0	0.0243	0.0		0.0020					5.6e+0
$\omega_{RS-4D-8}$		0.1698	0.0	0.0243	0.0	0.0	0.0020	0.0			0.0	5.6e+0
ω_{MR-4}		0.1698	0.0	0.0243			0.0020					5.6e+0
ω_{MR-5}		0.1698	0.0	0.0243			0.0020				0.0	5.6e+0
$\omega_{HN-m1-n0}$	0.0023	0.1183										5.6e+0
$\omega_{HN-m1-n1}$	0.0023	0.1183	0.0									5.6e+0
$\omega_{HN-m2-n0}$	0.0020	0.1170		0.0067								5.6e+0
$\omega_{HN-m2-n1}$	0.0020	0.1170	0.0	0.0067								5.6e+0
$\omega_{HN-m2-n2}$	0.0020	0.1170	0.0	0.0067		0.0						5.6e+0
$\omega_{HN-m3-n0}$	0.0005	0.1563		0.0198			0.0015					5.6e+0
$\omega_{HN-m3-n1}$	0.0005	0.1563	0.0	0.0198			0.0015					5.6e+0
$\omega_{HN-m3-n2}$	0.0020	0.1170	0.0	0.0067		0.0	0.0					5.6e+0

Table 5: Residuals of the objective function.

	Constitutive parameters determined for the uniaxial tests		Constitutive parameters determined for the confined tests	
	Uniaxial tests data	Confined tests data	Uniaxial tests data	Confined tests data
$\omega_{RS-1I-2}$	4.5e+1	2.1e+1	6.2e+1	1.6e+1
$\omega_{RS-2I-5}$	2.7e+1	1.5e+1	2.5e+2	5.7e+0
$\omega_{RS-3I-9}$	2.7e+1	1.4e+1	3.9e+2	5.6e+0
$\omega_{RS-1D-1}$	4.5e+1	2.0e+1	6.2e+1	1.6e+1
$\omega_{RS-2D-3}$	2.7e+1	2.3e+1	2.5e+2	5.7e+0
$\omega_{RS-3D-5}$	2.7e+1	1.5e+1	3.9e+2	5.6e+0
$\omega_{RS-4D-8}$	2.7e+1	1.5e+1	3.9e+2	5.6e+0
ω_{MR-4}	2.7e+1	2.3e+1	3.9e+2	5.6e+0
ω_{MR-5}	2.7e+1	2.3e+1	3.9e+2	5.6e+0
$\omega_{HN-m1-n0}$	2.8e+1	2.4e+1	4.1e+2	5.6e+0
$\omega_{HN-m1-n1}$	2.8e+1	2.4e+1	4.1e+2	5.6e+0
$\omega_{HN-m2-n0}$	2.7e+1	2.3e+1	3.9e+2	5.6e+0
$\omega_{HN-m2-n1}$	2.7e+1	2.3e+1	3.9e+2	5.6e+0
$\omega_{HN-m2-n2}$	2.7e+1	1.3e+1	3.9e+2	5.6e+0
$\omega_{HN-m3-n0}$	2.7e+1	2.3e+1	3.9e+2	5.6e+0
$\omega_{HN-m3-n1}$	2.7e+1	2.3e+1	3.9e+2	5.6e+0
$\omega_{HN-m3-n2}$	2.7e+1	1.3e+1	3.9e+2	5.6e+0

5 CONCLUSIONS

In this paper an experimental and numerical analysis of the elastic behaviour of Poly Vinyl Butyral (PVB) was performed, with reference to some particular stress states. This polymeric material, often used as interlayer in the laminated glass, plays a crucial role in the normal working and in the post crack behaviour of composite glass plates.

In this paper we reported some uniaxial and confined experimental tests, performed at room temperature, that highlighted the thermo-visco-elastic characteristics of the material. In this paper only the (conventional) elastic behaviour was taken in account. A best fitting procedure was implemented in order to determine the constitutive parameters relative to some well known polynomial hyperelastic potentials. It was apparent that low order terms are sufficient to fit the experimental data with an acceptable precision.

References

[1] Briccoli Bati, S., Fagone, M. and Ranocchiai, G., "The mechanical description of a rubber-like material for the evaluation of post-crack behaviour of laminated glass", in *Proc. XVIII Congresso dell'Associazione Italiana di Meccanica Teorica ed Applicata*, Brescia, Italy, September 11-14, 2007.

[2] Rivlin, R.S., and D.W. Saunders. "Large elastic deformations of isotropic materials VII. Experiments on the deformation of rubber." *Philosophical Transaction of the Royal Society of London Series A* 243, 251-288 (1951).

[3] Beatty, M.F. "Topics in finite elasticity: hyperelasticity of rubber, elastomers and biological tissues - with examples." *Appl. Mech. Rev.* 40, no. 12, 1699-1733 (1987).

[4] Hartmann, S., and P. Neff. "Polyconvexity of generalized polynomial-type hyperelastic strain energy functions for near-incompressibility." *International Journal of Solids and Structures* 40, 2767-2791, (2003).

[5] Ogden, R.W. "Large deformation isotropic elasticity - on the correlation theory and experiment for compressible rubber-like solids." *Proceedings of the Royal Society of London Series A* 328 (1972).

[6] James, A.G., A. Green, and G.M. Simpson. "Strain energy functions or rubber. I. Characterization of gum vulcanized." *Journal of applied polymer science* 19, 2033-2058, (1975).

[7] Treloar, L.R.G. *The Physics fo Rubber Elasticity*, Oxford University Press (1975).

[8] Arruda, M.C., and E.M. Boyce. "Constitutive models for rubber: a review." *Rubber Chem. Technol.* 73, 504-523 (2000).

[9] Drozdov, A.D. "Constitutive equations in finite elasticity of rubbers." *International Journal of Solids and Structures* 44, 272-297 (2007).

[10] Ogden, R.W. "Elements of the theory of finite elasticity." In Nonlinear elasticity, theory and applications, by Y.B. Fu and R.W. Ogden, 1-57. Cambridge university press, 2001.

[11] Diani, J., and M., Gilormini P. Brieu. "Observation and modeling of the anisotropic visco-hyperelastic behavior of a rubberlike material." *International Journal of Solids and Structures* 43, 3044-3056 (2006).

[12] Marsden, J.E., and T.J.R. Hughes. *Matematical foundations of elasticity*. New York: Dover Pubblications inc., (1983).

[13] Flory, P.J. "Thermodynamic relations for high elastic materials." *Transaction of the Faraday Society* 57, 829-838 (1961).